Bubble dynamics under the influence of the Marangoni force induced by a stratified field of contamination

Sadra Mahmoudi[1], Mahdi Saeedipour[2] (✉), Mark W. Hlawitschka[1] (✉)

1. Institute of Process Engineering, Johannes Kepler University Linz, Altenbergerstr. 69, 4040 Linz, Austria
2. Department of Particulate Flow Modelling, Johannes Kepler University Linz, Altenbergerstr. 69, 4040 Linz, Austria

Abstract

The Marangoni effect assumes significance in bubbly flows when temperature or concentration gradients exist in the domain. This study investigated the hydrodynamics of single bubbles under the influence of the Marangoni force induced by stratified fields of dissolved sugar, providing a numerical framework for examining these phenomena. A laboratory-scale bubble column and high-speed imaging were utilized to analyze the bubble behavior. The OpenFOAM-based geometric volume of the fluid solver was extended by incorporating the solutocapillary Marangoni effect, and a passive scalar transport equation for the sugar concentration was solved. The results revealed that small bubbles entering regions with elevated sugar concentrations experienced deceleration, transitioning into linear paths, while those departing from regions with high sugar concentrations exhibited fluctuations and meandering. Furthermore, the concentration gradient leads larger bubbles to meander throughout the entire column, without a notable increase in their velocity. The intensity of these behaviors is governed by the magnitude of the Marangoni force. The findings provide a better understanding of single bubble hydrodynamics in complex environments.

Keywords

bubble hydrodynamics
bubble column
Marangoni flow
liquid–gas flow
computational fluid dynamics

Article History

Received: 3 August 2023
Revised: 6 October 2023
Accepted: 25 November 2023

Research Article

1 Introduction

The accurate prediction of mass, momentum, and heat transfer across the liquid-gas interface is a fundamental concern in a great variety of industrial applications. Understanding the transport phenomena through a bubble interface hinges on gaining in-depth knowledge of single-bubble dynamics (Sieblist et al., 2011; Jo et al., 2016; Besagni et al., 2019; Mulbah et al., 2022). Understanding single bubble dynamics and how process parameters can affect the migration of bubbles has recently become an attractive field of research (Tripathi et al., 2015; Karimzadehkhouei et al., 2019; Mahmoudi et al., 2019, 2022; Cioncolini and Magnini, 2021; Kadivar et al., 2022; Mahmoudi and Hlawitschka, 2022). However, the behavior of bubbles in complex environments, such as contaminated environments, has been relatively less investigated. A small number of impurities that are not uniformly distributed can significantly alter bubble behavior. This phenomenon can be explained by local variations in fluid properties and the Marangoni effect. The Marangoni force, which stems from the surface tension gradient, causes the appearance of tangential shear stress on the bubble surface (Dukhin et al., 2016; Zhang et al., 2016). The Marangoni-induced flow, in which surface tension gradients play an important role in the behavior of bubbles, is the principal subject of this work. The Marangoni effect can become a potential parameter in bubbly flow in the presence of a temperature gradient (thermocapillarity) or concentration gradient (solutocapillarity) in the domain.

Thermocapillary convection is almost completely understood in actual and microgravity environments (e.g., drop towers, sounding rockets, and aboard space shuttles) and can be helpful in a myriad of pivotal applications for current and future life in microgravity areas, such as industrial, petroleum, and chemical engineering applications (Hetsroni et al., 2015; Jory and Satheesh, 2022). The Marangoni force can also stem from a surface tension gradient induced by the nonuniform distribution of impurities. In the case of

✉ M. Saeedipour, mahdi.saeedipour@jku.at; M. W. Hlawitschka, mark.hlawitschka@jku.at

Nomenclature

c	Concentration, % w/w
D_c	Diffusion coefficient, $m^2 \cdot s^{-1}$
d	Bubble equivalent diameter, m
$d_{b,max}$	Bubble largest diameter, m
$d_{b,min}$	Bubble smallest diameter, m
$\boldsymbol{F}_M$	Marangoni force, N
$\boldsymbol{F}_\sigma$	Surface tension force, N
$\dot{\boldsymbol{n}}$	Interface unit normal vector
p	Pressure, Pa
$\boldsymbol{U}$	Velocity vector, $m \cdot s^{-1}$

Subscriptions

b	Bubble
a	Air
w	Water

Greek symbols

α	Volume of fluid field
β	Surface tension dependence on the concentration
γ	Shear rate, s^{-1}
δ	Delta function, m^{-1}
κ	Interface curvature, m^{-1}
μ	Viscosity, Pa·s
ρ	Density, $kg \cdot m^{-3}$
σ	Surface tension, $N \cdot m^{-1}$
$\boldsymbol{\tau}$	Viscous stress tensor, Pa

surfactant impurities in the system, different studies have confirmed that the nonuniform distribution of surfactants decreases the surface tension and causes the retardation of interface motion, which in turn decreases the velocity of bubbles (Takagi et al., 2009; Takagi and Matsumoto, 2011). Although the effect of Marangoni forces induced by surfactants on bubble behavior is almost fully understood (Ulaganathan et al., 2014; Atasi et al., 2018; Zhang et al., 2022), the Marangoni forces induced by a stratified field of a specific impurity such as sugar have yet to be investigated. Our knowledge of the effects of a stratified field of a specific impurity on the single bubble dynamic characteristics, bubble–bubble interactions, and even the structure of the entire bubbly flow is still insufficient. These effects are of great importance in various technical and industrial applications, such as enhanced oil recovery, bubble-based microfluidics, froth flotation, and material synthesis (Li et al., 2012; Sun et al., 2014; Mahmoudi et al., 2017; Khalili Ata Abadi et al., 2023). In contrast to surfactant-laden flows, sugars increase water surface tension (in addition to altering other material properties, e.g., viscosity and density). Therefore, bubble behavior in such an environment may significantly differ from that in pure water or surfactant-laden media.

In the present study, numerical and experimental investigations are carried out on the effect of contamination on the shape and dynamics of a single bubble. Bubbles 4–8 mm in size were simulated in contaminated water with vertically positive and negative gradients of sugar concentrations corresponding to 0–40% w/w. The bubble shape, aspect ratio (AR), terminal velocity, and trajectory were studied. The influence of the surface tension dependence on the concentration on bubble behavior has also been studied. Such an in-depth understanding provides new insight for the interpretation of the large-scale characteristics of bubble column reactors under the influence of impurities.

2 Experimental methods and material properties

2.1 Experimental setup

The motion of bubbles was analyzed using the high-speed photography method in a column with a 22 cm height and a 5 cm × 5 cm cross section, which was filled with layers of sugar solution with different concentrations up to 20 cm. The experimental setup is shown in Fig. 1. The setup consisted of a rectangular tank, a gas supply, a light source, a high-speed camera, and a needle valve. A variable-size opening at the bottom of the column allows for the injection of gas at various flow rates and the generation of bubbles of various sizes. To create a stratified field of sugar concentration, layers of solutions with different concentrations were injected on top of each other. To capture high-quality images, the light source is located behind the column to provide sufficient illumination. The high-speed camera is mounted in front of the rectangular tank to capture bubble motion at a frame rate of 1000 images/s.

Figure 1 depicts the gradient of sugar concentration in the bubble column generated in the laboratory. The concentration gradient of the layers, which is used as the initial condition for the numerical simulations, is schematically shown in Fig. 2. The vertical positive gradient of sugar concentration, herein referred to as the positive concentration gradient, means that the concentration of sugar increases linearly from zero at the bottom of the column to 40% w/w in the uppermost part of the column. The vertical negative gradient of sugar concentration also means that the sugar concentration decreases from 40% w/w at the bottom of the

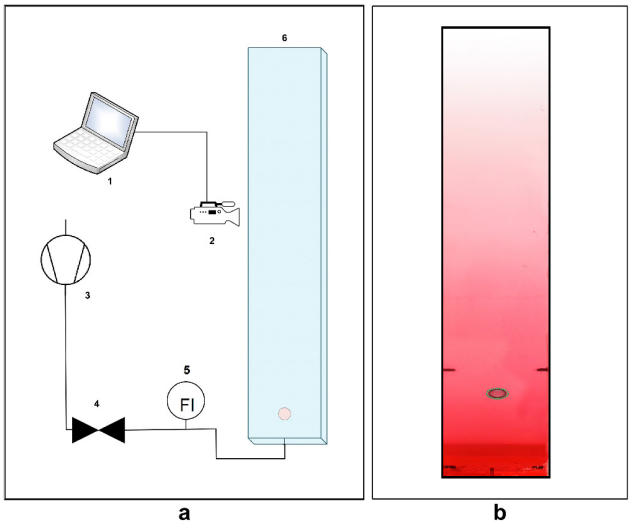

Fig. 1 (a) Experimental setup (1: software, 2: camera, 3: gas supply, 4: needle valve, 5: gas flow meter, 6: bubble column). (b) Generated negative concentration gradient in the laboratory.

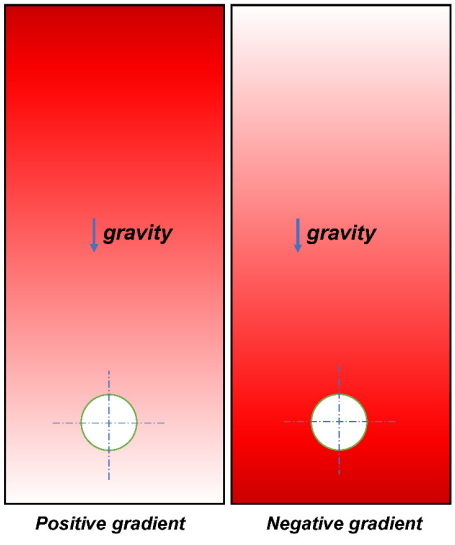

Fig. 2 Schematic illustration of the vertical variation in sugar concentration. The sugar concentration is denoted by the gradient in red.

column to zero in the uppermost part of the column. The sugar concentration varied from the highest (40% w/w) in the dark red part at the bottom of the column to zero in the colorless upper part of the column. Using the images of the high-speed camera, the bubble motion is captured, and the velocity, trajectory, and exact size of the bubble are measured via ImageJ software (Schindelin et al., 2012). The experiments were all carried out at atmospheric pressure and room temperature.

2.2 Material properties

Adding impurities to water can greatly affect its physical properties. The water surface tension, which is the focal parameter in the present study, increases with the dissolution of highly soluble impurities in water, while adding insoluble or sparingly soluble substances decreases the solution surface tension. Sugar is soluble in water and increases the surface tension of the solution exponentially, which causes the bubbly flow in such a medium to behave differently. Furthermore, adding sugar to water has the same effect on viscosity and density. The sugar solution properties, which are presented in Fig. 3, were extracted from the relevant literature and replotted (Ziegler et al., 1987; Ji et al., 2007; Telis et al., 2007; Price et al., 2016; Subbiah, 2018). To implement the solution properties in the developed code, the relevant correlations for each property were fitted using Origin Pro 2021 software.

3 Numerical simulation

3.1 Numerical model

The bubble hydrodynamics are numerically resolved by the VOF method. The governing equations of the two-phase interfacial flow of two immiscible fluids consist of the continuity and Navier–Stokes equations as well as a transport equation for the phase indicator function:

$$\frac{\partial \rho}{\partial t} + \nabla \cdot (\rho \boldsymbol{U}) = 0 \tag{1}$$

$$\frac{\partial (\rho \boldsymbol{U})}{\partial t} + \nabla \cdot (\rho \boldsymbol{U} \otimes \boldsymbol{U}) = -\nabla p + \rho \boldsymbol{g} + \nabla \cdot \boldsymbol{\tau} + \boldsymbol{F}_{\sigma} + \boldsymbol{F}_{\mathrm{M}} \tag{2}$$

$$\frac{\partial \alpha}{\partial t} + \nabla \cdot (\alpha \boldsymbol{U}) = 0 \tag{3}$$

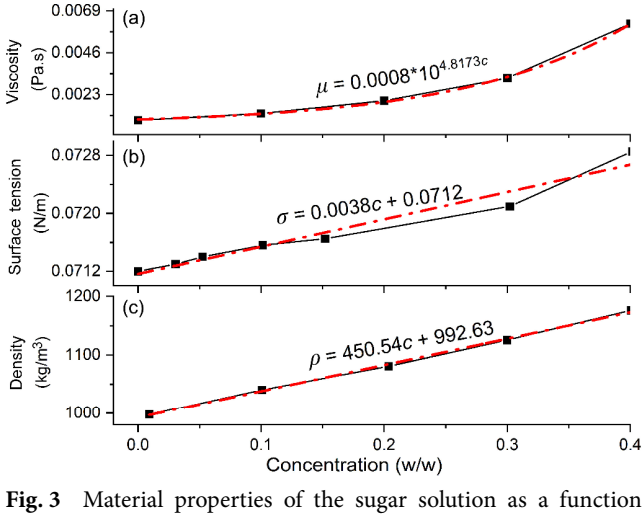

Fig. 3 Material properties of the sugar solution as a function of the sugar concentration c: (a) viscosity, (b) surface tension, (c) density.

In this one-fluid formulation, $\boldsymbol{U}$ is the velocity vector that is shared between the phases, p is the pressure, $\boldsymbol{g}$ is the gravitational acceleration vector, and $\boldsymbol{\tau} = \mu\left(\nabla \boldsymbol{U} + (\nabla \boldsymbol{U})^{\mathrm{T}}\right)$ is the viscous stress tensor. In addition, the volume fraction scalar field $\alpha = \frac{V_{\mathrm{air}}}{V_{\mathrm{cell}}}$ is transported to capture the liquid-gas interface, and the density and viscosity are determined based on the mixture assumption:

$$\rho = \alpha\rho_{\mathrm{a}} + (1-\alpha)\rho_{\mathrm{w}} \tag{4}$$

$$\mu = \alpha\mu_{\mathrm{a}} + (1-\alpha)\mu_{\mathrm{w}} \tag{5}$$

with subscripts a and w denoting air and water, respectively. $\boldsymbol{F}_{\sigma} = \sigma\kappa\hat{\boldsymbol{n}}\delta$ is the surface tension force, which is computed by the continuous surface force (CSF) method (Brackbill et al., 1992) based on the derivatives of the volume fraction, i.e., the interface unit normal vector $\hat{\boldsymbol{n}} = \frac{\nabla\alpha}{|\nabla\alpha|}$, and its curvature $\kappa = -\nabla\cdot\hat{\boldsymbol{n}}$. Here, σ is the surface tension coefficient, and $\delta \equiv |\nabla\alpha|$ is the delta function that equals infinity at the interface and zero elsewhere.

As an important mechanism in the present study, the Marangoni force caused by the surface tension gradient is modeled. In the context of finite volume CFD for interfacial flows with surface tension gradients due to temperature gradients (thermocapillarity) or concentration gradients (solutocapillarity), this force can be described by a tangential gradient operator (Saldi, 2012). In this study, with a focus on solutocapillarity and the assumption of soluble impurities in water, the Marangoni force reads

$$\boldsymbol{F}_{\mathrm{M}} = \beta[\nabla c - \hat{\boldsymbol{n}}(\hat{\boldsymbol{n}}\cdot\nabla c)]|\nabla\alpha| \tag{6}$$

where c is the concentration of the impurity, and a passive scalar transport equation is solved exclusively in the liquid phase:

$$\frac{\partial c}{\partial t} + \nabla\cdot(c\boldsymbol{U}) = D_{\mathrm{c}}\nabla^2 c \tag{7}$$

Here, D_{c} is the diffusion coefficient for impurities in water. In addition, Eq. (6) contains the surface tension dependence on the concentration $\beta = \frac{\mathrm{d}\sigma}{\mathrm{d}c}$, which, in addition to the diffusion coefficient, density, and viscosity of sugar, are extracted from the available experimental works (Ziegler et al., 1987; Ji et al., 2007; Telis et al., 2007; Price et al., 2016; Subbiah, 2018). In the context of finite volume CFD, the numerical solution of the described system of equations is supposed to resolve the bubble dynamics in the presence of contaminated water. Numerical simulations were performed with OpenFOAM using the geometric VOF method of IsoAdvector (Roenby et al., 2016) for interface capture and a PISO-like algorithm for pressure-velocity coupling (Weller et al., 1998).

3.2 Simulation setup

The simulations were performed on a three-dimensional computational domain representing a wall-bounded, open-top, rectangular tank with H = 0.2 m and L = 0.04 m, as schematically shown in Fig. 4. The domain is filled with water, and a 3D air bubble is initialized inside the domain with the centroid located at (L/2, H/10). Gravity is set to $\vec{\boldsymbol{g}}$ (0, −9.81, 0) to initiate buoyancy-driven upward motion of the bubble at the beginning of the simulation. The material properties are initially set according to the standard conditions (ρ_{w} = 1000 kg·m^{-3}, ρ_{a} = 1.18 kg·m^{-3}, μ_{w} = 8.9×10^{-4} Pa·s, and μ_{a} = 1.77×10^{-5} Pa·s), and the surface tension coefficient is σ = 0.0712 N·m^{-1}.

To reproduce the sugar concentration gradient field in water as explained in the experiment, the passive scalar field of c is initialized with a linear rate in the vertical direction, and the physical properties of the continuous phase are accordingly linked to the concentration value. It is worth mentioning that an OpenFOAM function object called *phaseScalarTransport* is adopted to prevent the penetration of contaminants into the bubble during the simulation, i.e., the contamination field is only transported inside the water phase. The dependency of the surface tension on the concentration (β) is unique for each system and is equal to 0.0038 in the case of an aqueous sugar solution ($c \le 0.4$ w/w). To obtain insight into the influence of β on bubble behavior with the aid of CFD, three different values were assigned to this parameter (β = 0.2, 0.02, 0.0038, and 0), among which 0.2, 0.02, and 0 are

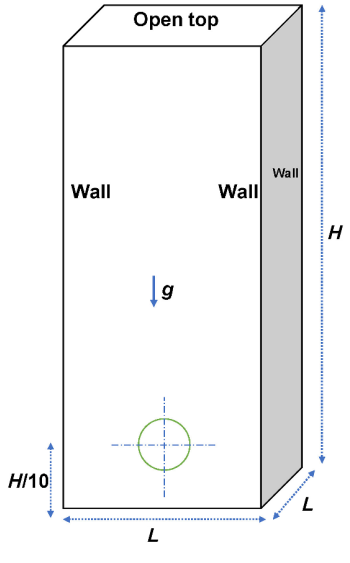

Fig. 4 Schematics of the computational domain.

artificial values. To exclusively study the influence of the Marangoni force on bubble behavior, the artificial cases of $\beta = 0$, in which the concentration gradient is applied but the Marangoni force is manually set to zero, were considered. The mass diffusivity coefficient (D_c) of sugar in water was considered to be 5×10^{-10} $m^2 \cdot s^{-1}$ (Cardoso Andrade et al., 2007).

The free slip wall assumption is imposed for the velocity vector at the confining walls (parallel to the flow), whereas the open boundary at the top of the domain is subjected to atmospheric pressure. The simulation boundary conditions for the pressure, velocity, and volume fraction fields as well as the passive scalar are summarized in Table 1.

In the context of geometric VOF of the IsoAdvector method, a plic-RDF scheme is employed for the reconstruction of the interface from a discretized volume fraction (Scheufler and Roenby, 2019). This scheme has shown better performance in the prediction of the interface curvature in previous studies (Gamet et al., 2020; Saeedipour and Schneiderbauer, 2021). The simulations were carried out using adaptive time steps, where the time step size was limited by a maximum Courant number of 0.01. Preliminary simulations (not presented here) have revealed that such a low Courant number is necessary for accurate prediction of the bubble rising velocity. For more information about the numerical simulation setup and details on the geometric VOF simulation, we refer to previous works (Gamet et al., 2020; Saeedipour et al., 2021). In terms of velocity and bubble trajectory analysis, a systematic procedure was devised to compute the velocity of the secondary phase and to track the center of mass of individual bubbles. Furthermore, by employing image processing techniques, snapshots of the bubbles were subjected to detailed examination to determine their respective maximum and minimum diameters ($AR = d_{b,min} / d_{b,max}$). To ensure precise measurement of the AR, two snapshots of each bubble, obtained from different viewpoints, specifically from the *XY*-plane and *YZ*-plane, were analyzed at every time step.

3.3 Grid independence study

The domain was discretized with equidistant computational cells at three different resolutions of 1: *L*/100, 2: *L*/140, 3: *L*/180, and one case with a dynamic mesh of 4: *L*/140 in the balk flow with three-level recursive refinements at the interface. An air bubble (d = 4 mm) was released in the center of the column at a height of 10 mm. The instant bubble velocity is used as the measure for the grid independence study. As shown in Fig. 5, the results show grid convergence for the third and fourth grid resolutions, as the difference between their results is less than 5%, which is within an acceptable range (Cioncolini and Magnini, 2021). A grid size of *L*/140 with three levels of refinements was chosen for this study to prevent higher computational costs.

4 Results and discussion

First, in a case study, the simulation results are compared to the experimental results. The experiments are limited by variations in sugar concentration and gradient; therefore, a purely numerical study was performed to investigate the behavior (shape fluctuations, velocity, and trajectory) of 4 mm, 6 mm, and 8 mm bubbles in the presence of a gradient of sugar concentrations and under the influence of different magnitudes of the Marangoni force.

4.1 Validation study: experiment vs. simulation

To validate the numerical model, a comparison was made between the bubble trajectory and terminal velocity obtained from the simulations and the corresponding experimental data. Figure 6 illustrates the trajectory of a 4.5 mm bubble in a sugar solution. The trajectory of the 4.5 mm bubble in the sugar solution, as observed in the experimental data, closely aligns with its counterpart obtained through numerical simulation. Under the influence of a negative concentration gradient, where a higher sugar concentration is present at the bottom and a lower concentration is present at the top, the 4.5 mm bubble exhibits a linear path in both the experimental and numerical cases until reaching the middle of the column. Subsequently, it gradually begins to meander, with zigzag movements becoming more prominent. The trajectories obtained from both sets of results exhibit strong similarity, indicating that the developed and applied solver in this study reliably predicts the bubble trajectory in both pure and contaminated media.

Figure 7 illustrates a comprehensive comparison between the numerical and experimental average velocities of 2 mm, 3 mm, 4 mm, and 5 mm bubbles within an aqueous sugar solution featuring a negative gradient. The observed deviation

Table 1 Boundary conditions for different variables in the OpenFOAM simulation

Boundary	Pressure p	Velocity U	Volume fraction α	Contamination field c
Walls	fixedFluxPressure	slip	zeroGradient	zeroGradient
Top boundary	totalPressure	pressureInletOutletVelocity	inletOutlet	zeroGradient

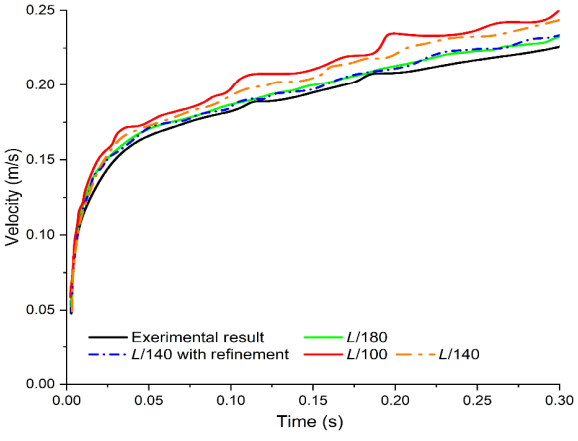

Fig. 5 Grid independence study: the increase in a single bubble of 4 mm in a negative gradient of sugar solution for different grid resolutions in comparison with experimental measurements.

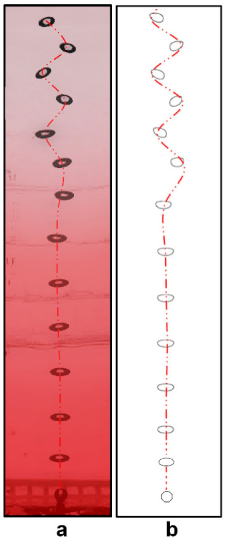

Fig. 6 Series of close-up images of a 4.5 mm bubble: (a) experiment and (b) simulation with $\beta = 0.0038$.

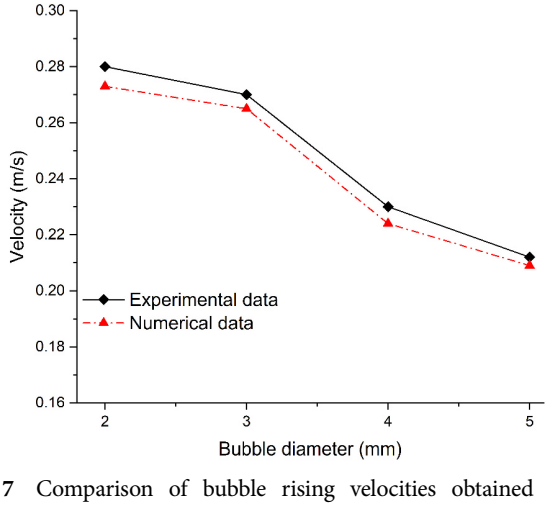

Fig. 7 Comparison of bubble rising velocities obtained from experiments and simulations for different bubble diameters (2 mm, 3 mm, 4 mm, and 5 mm).

remains below 5%, underscoring the exceptional accuracy of the utilized model in predicting bubble behavior within intricate environments. Notably, smaller bubbles exhibit a greater deviation, which can be attributed to their greater deformation and zigzag-like trajectories during motion.

Figure 8 presents the contour of the sugar distribution throughout the entire column as an 8 mm bubble ascends in an aqueous sugar solution ($\beta = 0.0038$). The sugar concentration on the tail of the bubble was consistently greater than that in other areas in close proximity to the bubble surface. This observation underscores the vertical transport of sugar, facilitated by the convection mechanism induced by bubble movement. This phenomenon was also distinctly observed in the experiments. Notably, the transport of sugar by bubbles results in the Marangoni force attaining its maximum magnitude on the lower part of the bubble surface.

4.2 Hydrodynamics of single bubbles

Figures 9 and 10 show the simulation results for the 4 mm bubble terminal velocity and AR, respectively. In the case of a positive concentration gradient (Fig. 9(a)), the bubbles encounter a lower Marangoni force at the beginning, and the bubble behavior in terms of velocity and AR resembles that in pure water. In this case, the bubble moves upward in the lower part of the column in a zigzag path. The low viscosity of the liquid causes the bubble to have a fluctuating shape, which causes the drag force and instant velocity to fluctuate. In addition, after 0.5 s, when the bubble reaches the upper part of the column, it encounters greater Marangoni and viscous forces, which together increase the AR (Fig. 10(a)),

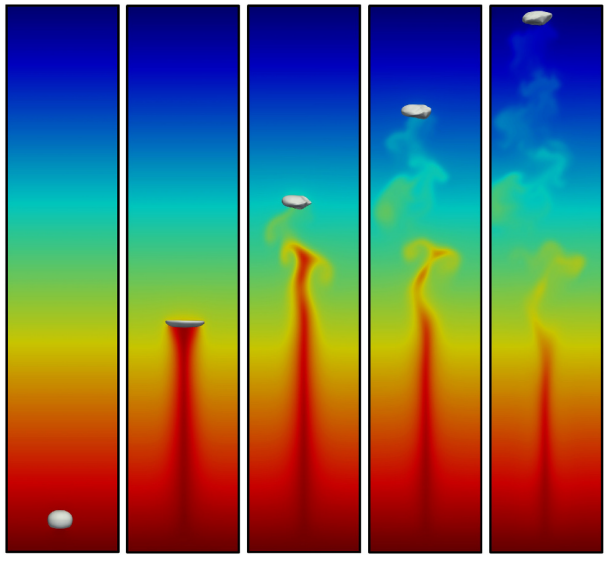

Fig. 8 Contour of sugar concentration around and in the wake of an 8 mm bubble when it rises in the water column (red - high concentration, blue - low concentration).

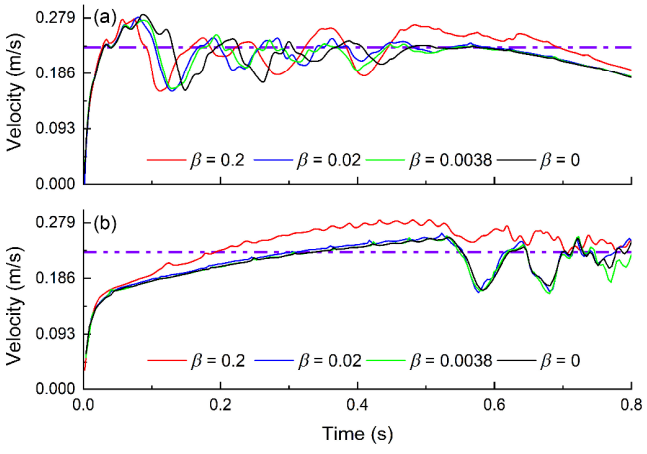

Fig. 9 Velocity of 4 mm bubbles at different concentration gradients: (a) positive and (b) negative gradients. The simulation results for different β values are compared. The horizontal dashed-dotted line represents the average velocity of the 4 mm bubble in pure water.

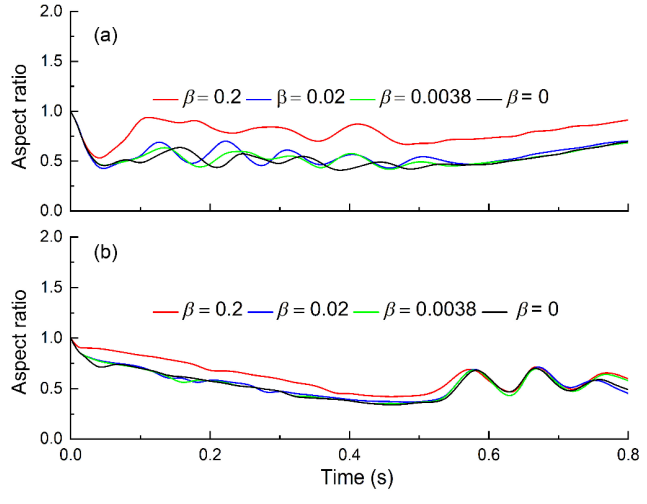

Fig. 10 Aspect ratio of 4 mm bubbles in (a) vertical positive and (b) vertical negative gradients of sugar concentration.

and it approaches unity (which contributes to the velocity increase). Furthermore, from 0.5 onward, under the influence of viscous forces, which dampen the velocity fluctuations, the bubble starts to move in a rectilinear path (Fig. 11). As this bubble is in the so-called viscous force dominant regime, the viscous forces overcome the increment effects resulting from the AR increment and rectilinear movement. From this point onward (t = 0.5 s), the bubbles experience a slowdown, and they move up at a lower velocity.

The β determines the strength of the Marangoni force in the domain. A high β generates a strong Marangoni force, which, in turn, contributes to the zigzag motion and increase in the AR. In the case of a positive concentration gradient, a noticeable increase in the β value increases the AR throughout the whole column, while it increases the deviation and zigzag behavior of bubbles only in the lower section of the column. Therefore, increasing β increases the bubble velocity in the upper section of the column where the aforementioned forces do not balance each other.

In the case of a negative concentration gradient (Fig. 9(b) and Fig. 10(b)), bubbles in the lower part of the column are exposed to high Marangoni forces, which dampen the AR oscillations (Fig. 10(b)). In this case, the AR decreases gradually to reach a stable state. The presence of a strong resistance force overcomes the Marangoni force and prevents bubbles from meandering. As the concentration decreases linearly in the upward direction, the dominant viscous forces gradually decrease, which causes the bubble to accelerate in the lower section of the column. When the bubbles reach the upper part of the column, the Marangoni force and weaker viscous forces cause the bubbles to meander and have fluctuating velocities and ARs.

In the case of a negative concentration gradient, the value of β does not intensify the zigzag behavior of the bubble trajectory (Fig. 11), but it affects the bubble velocity and AR. Higher values of β have a discernible impact on the AR in the lower section of the column, although they do not significantly influence the intensity of the zigzag motion. Consequently, higher β values lead to increased bubble velocity in the lower section of the column while exerting a relatively weaker effect on the velocity of bubbles in the upper section.

As Fig. 12(a) shows, the 6 mm bubble, compared to the 4 mm bubble, does not decelerate when it enters the area with a higher concentration. In the case of a positive concentration gradient, the bubble's velocity remains relatively unchanged (compared to the velocity of the same bubble in pure water) in the lower section of the column as

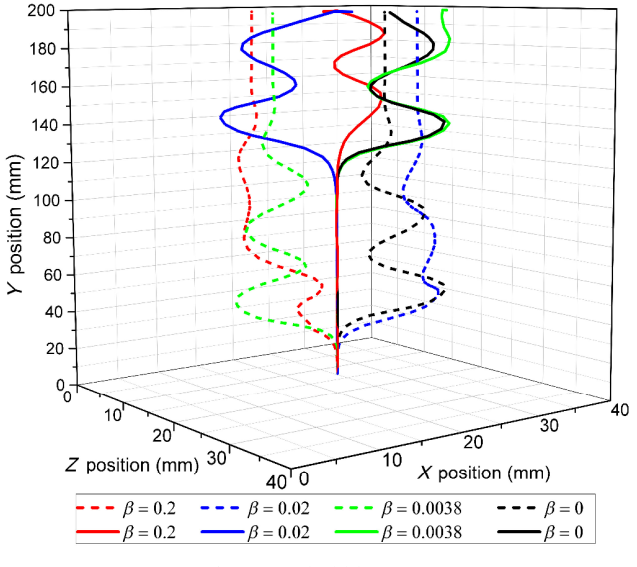

Fig. 11 Trajectory of 4 mm bubble in positive concentration gradient (dash-dotted lines) and negative concentration gradient (solid lines) simulated with different β values.

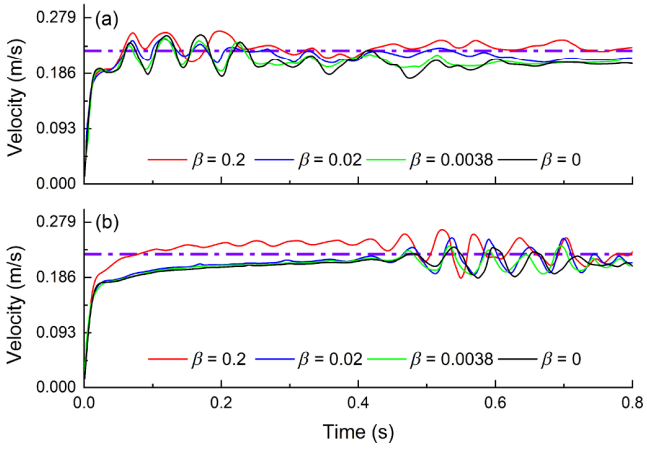

Fig. 12 Velocity of 6 mm bubbles in (a) vertical positive and (b) vertical negative gradients of sugar concentration. The horizontal dashed-dotted line represents the average velocity of the 6 mm bubble in pure water.

the AR increment effect and zigzag motion effect (resulting from the Marangoni force) balance each other (Fig. 13(a) and Fig. 14). The aspect ratio of the bubble, as shown in 13(a), experiences noticeable fluctuations in the lower section of the column where the Marangoni force and viscous forces are minimized. In this area, the bubble has a zigzag behavior, and a higher Marangoni force intensifies the zigzag behavior. The zigzag behavior and AR increment of the 6 mm bubble are less pronounced than those of the 4 mm bubble in the same liquid. Upon reaching the area with a higher sugar concentration after 0.5 s, the viscous forces mitigate the fluctuation in the AR and reduce the intensity of the bubble zigzag behavior. However, the shear rate acting on a 6 mm bubble, stemming from the Marangoni force, prevents the weaker viscous force from compelling the bubble to assume a rectilinear path, similar to that observed in the case of a 4 mm bubble. Consequently, in

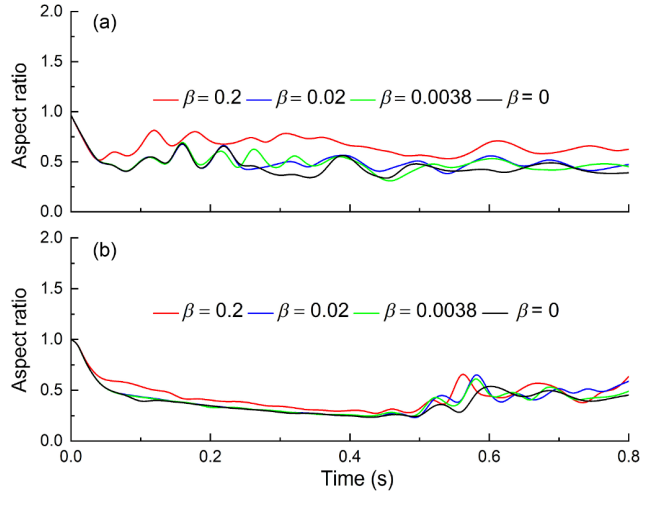

Fig. 13 Aspect ratio of 6 mm bubbles in (a) vertical positive and (b) vertical negative gradients of sugar concentration.

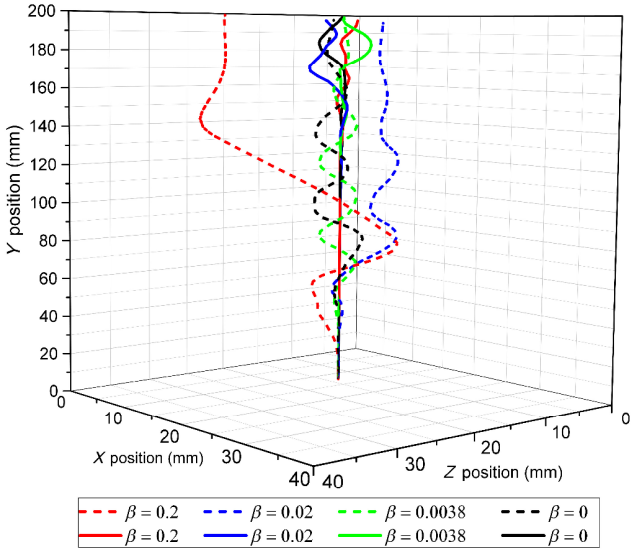

Fig. 14 Trajectories of a 6 mm bubble under a positive concentration gradient (dashed dotted lines) and a negative concentration gradient (solid lines) simulated with different β values.

the upper section of the column, the bubble maintains its average velocity without decelerating upon reaching the area of high concentration.

In the case of the 6 mm bubble in the positive concentration gradient, a considerable increase in the β value increases the AR throughout the whole column, while it increases the deviation and zigzag behavior of the bubble in the lower and middle sections of the column. Therefore, increasing β increases the bubble velocity in the upper section of the column as the zigzag behavior and AR increase neutralize each other in the middle and lower sections of the column. Interestingly, the magnitude of β also affects the starting point of tumbling. In fact, higher values of β generate stronger Marangoni forces, which cause them to tumble at lower heights of the column.

The behavior of a 6 mm bubble in a negative concentration gradient closely resembles that of a 4 mm bubble in the same situation. The notable difference lies in the fact that the 6 mm bubble in the lower section of the column does not experience acceleration. This difference stems from the fact that the larger bubbles are in the so-called surface tension force dominant regime, which prevents them from being sensitive to viscosity variation. Another difference in the upper section of the column is that the lower shear rate stems from the Marangoni force, which acts on the 6 mm bubble surface to prevent the bubble from meandering as severely as a 4 mm bubble. In fact, the shear rate acting on a bubble surface and bubble size are inversely correlated as $\dot{\gamma} \propto \left(\frac{1}{d_b}, \boldsymbol{U}_b\right)$, where $\boldsymbol{U}_b$ is the bubble velocity and d_b is the bubble diameter. Therefore,

the rate of shear acting on the bubble surface is inversely proportional to the bubble size. Therefore, the 4 mm bubbles are exposed to a stronger shear rate, which causes them to follow a more zigzag pattern, while the 6 mm bubble movements are even more central than the trajectory of a 6 mm bubble in pure water, which deviates slightly to the walls of the column.

Under a negative concentration gradient, the value of β does not amplify the zigzag behavior of the bubble (Fig. 14); however, it does result in increased bubble AR and velocity in the lower section of the column.

The behavior of the 8 mm bubble varies among the simulated cases in this study, depending on the direction of the concentration gradient, primarily due to its larger surface area and more pronounced deformations. As depicted in Fig. 15(a), the Marangoni force resulting from the positive concentration gradient does not exert a discernible influence on the bubble's velocity. Notably, the effects of the AR and trajectory (Fig. 16(a) and Fig. 17) offset each other throughout

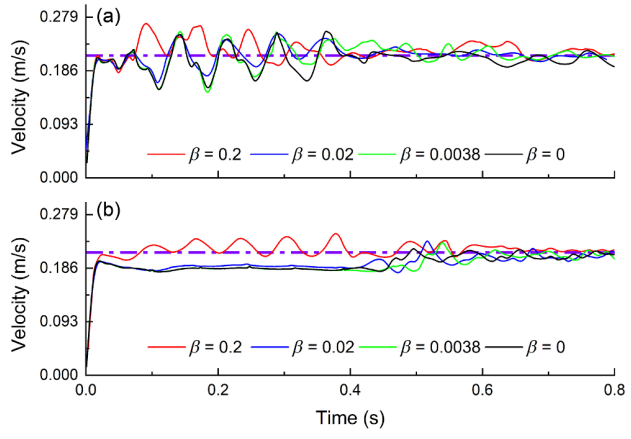

Fig. 15 Velocity of 8 mm bubbles in (a) vertical positive and (b) vertical negative gradients of sugar concentration. The horizontal dashed-dotted line represents the average velocity of the 8 mm bubble in pure water.

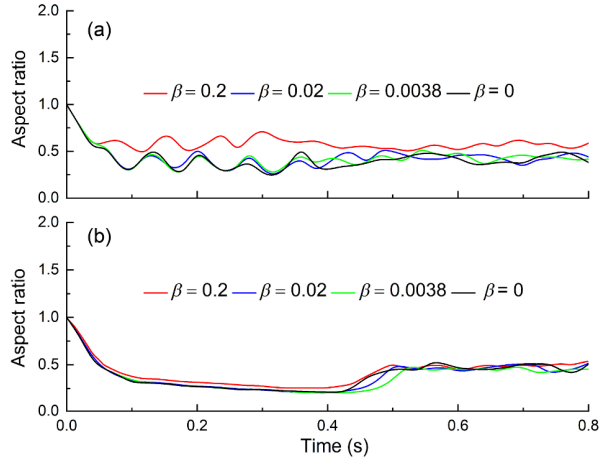

Fig. 16 Aspect ratio of 8 mm bubbles in (a) vertical positive and (b) vertical negative gradients of sugar concentration.

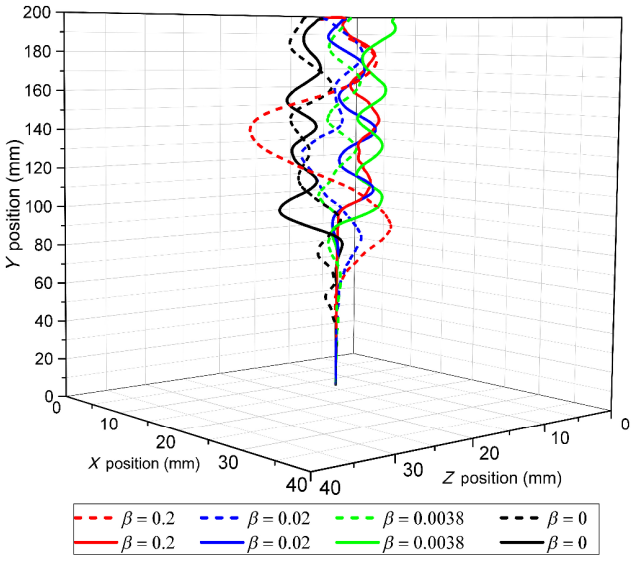

Fig. 17 Trajectory of an 8 mm bubble in a positive concentration gradient (dashed-dotted lines) and negative concentration gradient (solid lines) simulated with different β values.

the column. Consequently, increasing the β value does not lead to a higher velocity for the 8 mm bubble, unlike for the 4 mm and 6 mm bubbles. Similar to the 4 mm and 6 mm bubbles, the 8 mm bubble experiences an augmented AR throughout the column as a result of increasing the β value. However, unlike the 4 mm and 6 mm bubbles that follow straight paths in the upper section of the column, the 8 mm bubble moves in a zigzag trajectory as it rises, making it less affected by changes in β.

The 8 mm bubbles within the negative concentration gradient exhibit a distinct behavior compared to the 4 mm and 6 mm bubbles. In fact, the 8 mm bubble does not tumble within the denser region but instead initiates tumbling at a lower height. Consequently, the behavior of the 8 mm bubble appears similar to that of the 4 mm and 6 mm bubbles, albeit with a notable difference—the 8 mm bubble experiences no acceleration in the lower section of the column, unlike the other two bubbles. Furthermore, despite a more potent Marangoni force, this force does not significantly influence the trajectory of the 8 mm bubble; however, it does increase the AR of the bubble in the lower section of the column.

As Fig. 18 shows, in the case of a negative concentration gradient, the sugar concentration in the upper region of the bubble surface is lower than that in the lower region of the bubble surface. Consequently, this concentration gradient along the surface induces a Marangoni flow from the region of lower surface tension toward the region of higher surface tension, localized exclusively at the interface. The presence of this flow significantly influences the sphericity of the bubbles and subsequently impacts their velocity. Figure 19 also depicts the same mechanism in the case of a positive concentration gradient.

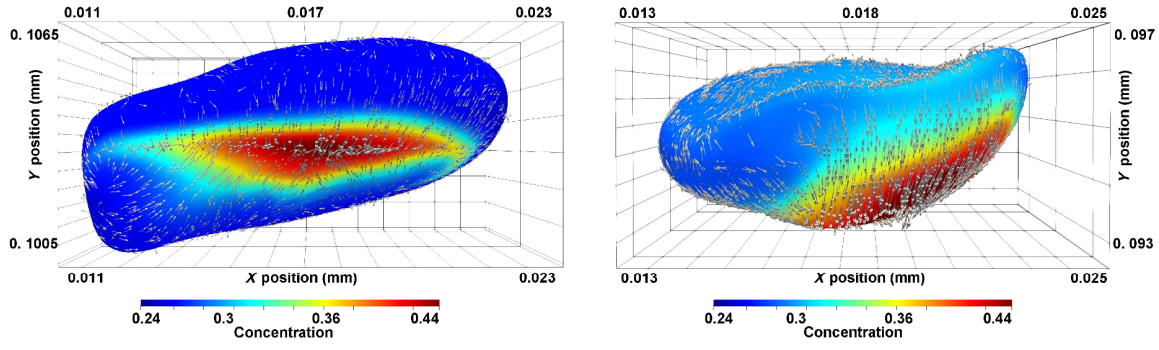

Fig. 18 Contamination distribution on the 8 mm bubble surface under a negative concentration gradient ($\beta = 0.02$) at $t = 0.5$ s and $t = 0.45$ s . The white arrows represent the Marangoni force ($\boldsymbol{F}_{\mathrm{M}}$).

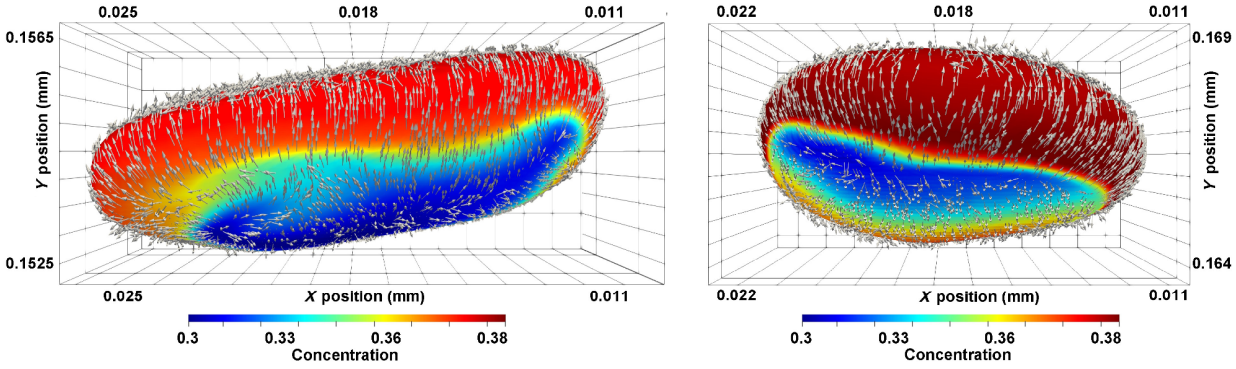

Fig. 19 Contamination distribution on the 8 mm bubble surface in a positive concentration gradient ($\beta = 0.02$) at $t = 0.7$ s and $t = 0.76$ s . The white arrows represent the Marangoni force ($\boldsymbol{F}_{\mathrm{M}}$).

5 Conclusions

This study focused on the influence of sugar solution gradients using CFD simulations, taking into account Marangoni forces. A systematic approach was adopted to calculate the velocity of the secondary phase and track the center of mass of the bubbles. Employing image processing techniques, bubble snapshots were analyzed to determine their aspect ratio from two different viewpoints at each time step. The results of the developed solver were compared to experimental data, and then, the solver was used to investigate the systems involving both negative and positive concentration gradients.

The velocity of bubbles is directly proportional to the surface tension and is inversely proportional to the liquid viscosity, i.e., $U_{\mathrm{b}} \propto \left(\frac{1}{\mu}, \sigma\right)$. Consequently, impurities that can induce more pronounced changes in these parameters will correspondingly impact the bubble velocity. For instance, the addition of surfactants to a bubble column is known to decrease the bubble terminal velocity by reducing the surface tension and immobilization of the interface as well as increasing the viscosity (Takagi et al., 2009; Takagi and Matsumoto, 2011). However, in the case of an impurity such as sugar, which simultaneously increases both viscosity and surface tension, the augmenting effect of surface tension on bubble velocity can be counterbalanced by the diminishing effect of viscosity. Therefore, if the added impurity significantly alters the surface tension ($\beta \geq 0.2$), it can overcome the decreasing impact of viscosity on bubble velocity, leading to an acceleration of the bubbles.

Upon the entry of 4 mm bubbles into regions of elevated sugar concentration, the bubbles undergo deceleration, transitioning into a linear path. Conversely, when 4 mm bubbles depart from high sugar concentration areas, they meander, and their velocity fluctuates. The intensity of this behavior depends on the value of β, which determines the magnitude of the Marangoni force. For the bubble velocity, increasing β leads to a higher bubble velocity when the impurity concentration exceeds 20% w/w. In both the positive and negative cases, higher β values result in higher ARs, leading to reduced drag forces and, consequently, higher velocities. In the context of a negative concentration gradient, the magnitude of β has no discernible impact on the trajectory of the 4 mm bubbles. However, in the case of a positive concentration gradient, higher values of β intensify the zigzag motion of bubbles in the lower section of the column. Under a positive concentration gradient, 6 mm bubbles do not exhibit pronounced zigzag trajectories and experience no significant slowdown upon entering the

concentrated area of the column. The presence of tangential forces and a downward liquid flow causes the bubbles to deviate toward the walls. In such cases, higher values of β generate stronger Marangoni forces, leading to the tumbling of bubbles at lower heights within the column. On the other hand, under a negative concentration gradient, the behavior of the 6 mm bubbles resembles that of the 4 mm bubbles. The primary difference lies in the milder meandering path observed in the 6 mm bubbles. Moreover, 6 mm bubbles exhibit reduced sensitivity to alterations in viscous forces in comparison to 4 mm bubbles. For 8 mm bubbles, a positive concentration gradient has minimal influence, whereas under a negative gradient, the bubbles experience acceleration upon reaching areas of lower concentration.

This study revealed that the influence of the β magnitude increases the AR throughout the column and enhances the zigzag behavior in cases with positive concentration gradients where β is less than 20% w/w. Consequently, the velocity increases when the impurity concentration exceeds 20% w/w. Therefore, impurities causing a substantial increase in surface tension result in higher average bubble velocities, which is potentially unfavorable for prolonging the contact time between the two phases. Conversely, impurities that decrease or only slightly increase surface tension induce meandering behavior and reduce bubble speed, extending the contact time between phases and ensuring a higher mass transfer rate. The presence of a concentration gradient effectively promotes mixing and intensifies turbulence through interactions with larger bubbles, thereby enhancing mass transfer and directing the column flow regime toward transient and heterogeneous flow regimes. In all cases, smaller bubbles exhibit meandering behavior in specific parts of the column, whereas the concentration gradient leads larger bubbles to meander throughout the entire column without a notable increase in their velocity.

Finally, the introduction of impurities causing substantial changes in surface tension results in profoundly distinct behaviors in individual bubbles, as well as in bubble clusters and bubbly flows. Future research prospects involve the development of a novel solver and the design of an innovative experimental setup to investigate the effects of different concentrations of the intended impurity within the current system. Such investigations offer valuable opportunities to enhance the understanding of bubble dynamics in the presence of various impurities and their implications for multiphase flow phenomena.

Funding note

Open access funding provided by Johannes Kepler University Linz.

Declaration of competing interest

The authors have no competing interests to declare that are relevant to the content of this article.

References

Atasi, O., Haut, B., Pedrono, A., Scheid, B., Legendre, D. 2018. Influence of soluble surfactants and deformation on the dynamics of centered bubbles in cylindrical microchannels. *Langmuir*, 34: 10048–10062.

Besagni, G., Gallazzini, L., Inzoli, F. 2019. On the scale-up criteria for bubble columns. *Petroleum*, 5: 114–122.

Brackbill, J. U., Kothe, D. B., Zemach, C. 1992. A continuum method for modeling surface tension. *Journal of Computational Physics*, 100: 335–354.

Cardoso Andrade, S. A., de Barros Neto, B., Cavalcanti Nóbrega, A., Moreira Azoubel, P., Barbosa Guerra, N. 2007. Evaluation of water and sucrose diffusion coefficients during osmotic dehydration of jenipapo (Genipa Americana L.). *Journal of Food Engineering*, 78: 551–555.

Cioncolini, A., Magnini, M. 2021. Shapes and rise velocities of single bubbles in a confined annular channel: Experiments and numerical simulations. *Fluids*, 6: 437.

Dukhin, S. S., Lotfi, M., Kovalchuk, V. I., Bastani, D., Miller, R. 2016. Dynamics of rear stagnant cap formation at the surface of rising bubbles in surfactant solutions at large Reynolds and Marangoni numbers and for slow sorption kinetics. *Colloids and Surfaces A: Physicochemical and Engineering Aspects*, 492: 127–137.

Gamet, L., Scala, M., Roenby, J., Scheufler, H., Pierson, J. L. 2020. Validation of volume-of-fluid OpenFOAM® isoAdvector solvers using single bubble benchmarks. *Computers & Fluids*, 213: 104722.

Hetsroni, G., Mosyak, A., Pogrebnyak, E. 2015. Effect of Marangoni flow on subcooled pool boiling on micro-scale and macro-scale heaters in water and surfactant solutions. *International Journal of Heat and Mass Transfer*, 89: 425–432.

Ji, P., Feng, W., Tan, T. 2007. Density calculation of sugar solutions with the SAFT model. *Journal of Chemical & Engineering Data*, 52: 135–140.

Jo, H., Park, H. S., Kim, M. H. 2016. Single bubble dynamics on hydrophobic–hydrophilic mixed surfaces. *International Journal of Heat and Mass Transfer*, 93: 554–565.

Jory, K., Satheesh, A. 2022. Marangoni convection in shallow annular pools of silicone oil heated from above. *Case Studies in Thermal Engineering*, 40: 102556.

Kadivar, E., el Moctar, O., Sagar, H. J. 2022. Experimental study of the influence of mesoscale surface structuring on single bubble dynamics. *Ocean Engineering*, 260: 111892.

Karimzadehkhouei, M., Özbey, A., MacKenzie-Dover, C., Christy, J. R. E., Sefiane, K., Koşar, A. 2019. Investigation of single air bubble dynamics and the effect of nanoparticles in rectangular minichannels. *Journal of Molecular Liquids*, 279: 510–517.

Khalili Ata Abadi, P., Vaziri Naeen Nejad, J., Kheradmand, S., Khalili Ata Abadi, D. 2023. A dimensional optimization study on cyclone performance under the oscillating boundary condition.

Chemical Engineering and Processing - Process Intensification, 183: 109217.

Li, Y., Zhu, T., Liu, Y., Tian, Y., Wang, H. 2012. Effects of surfactant on bubble hydrodynamic behavior under flotation-related conditions in wastewater. *Water Science and Technology*, 65: 1060–1066.

Mahmoudi, S., Hashemi Shahraki, B., Aghajani, M. 2017. Correction of terminal velocity prediction model for CO_2-kerosene and air-kerosene systems by artificial intelligence. *Software Engineering* (*Science Publishing Group*), 5: 65.

Mahmoudi, S., Hashemi Shahraki, B., Aghajani, M. 2019. Experimental and theoretical investigation of CO_2 and air bubble rising velocity through kerosene and distilled water in bubble column. *Journal of Dispersion Science and Technology*, 40: 33–42.

Mahmoudi, S., Hemmatian, F., Dahkaee, K. P., Hlawitschka, M. W., Kantzas, A. 2022. Detailed study of single bubble behavior and drag correlations in Newtonian and non-Newtonian liquids for the design of bubble columns. *Chemical Engineering Research and Design*, 179: 119–129.

Mahmoudi, S., Hlawitschka, M. W. 2022. Effect of solid particles on the slurry bubble columns behavior—A review. *ChemBioEng Reviews*, 9: 63–92.

Mulbah, C., Kang, C., Mao, N., Zhang, W., Shaikh, A. R., Teng, S. 2022. A review of VOF methods for simulating bubble dynamics. *Progress in Nuclear Energy*, 154: 104478.

Price, H. C., Mattsson, J., Murray, B. J. 2016. Sucrose diffusion in aqueous solution. *Physical Chemistry Chemical Physics*, 18: 19207–19216.

Roenby, J., Bredmose, H., Jasak, H. 2016. A computational method for sharp interface advection. *Royal Society Open Science*, 3: 160405.

Saeedipour, M., Schneiderbauer, S. 2021. Favre-filtered LES-VOF of two-phase flows with eddy viscosity-based subgrid closure models: An a-posteriori analysis. *International Journal of Multiphase Flow*, 144: 103780.

Saeedipour, M., Vincent, S., Estivalezes, J. L. 2021. Toward a fully resolved volume of fluid simulation of the phase inversion problem. *Acta Mechanica*, 232: 2695–2714.

Saldi, Z. 2012. Marangoni driven free surface flows in liquid weld pools. Delft University of Technology, the Netherlands.

Scheufler, H., Roenby, J. 2019. Accurate and efficient surface reconstruction from volume fraction data on general meshes. *Journal of Computational Physics*, 383: 1–23.

Schindelin, J., Arganda-Carreras, I., Frise, E., Kaynig, V., Longair, M., Pietzsch, T., Preibisch, S., Rueden, C., Saalfeld, S., Schmid, B., et al. 2012. Fiji: An open-source platform for biological-image analysis. *Nature Methods*, 9: 676–682.

Sieblist, C., Jenzsch, M., Pohlscheidt, M., Lübbert, A. 2011. Bioreactor fluid dynamics. In: *Comprehensive Biotechnology*. Amsterdam: Elsevier, 47–62.

Subbiah, B. 2018. Physical properties of simple and complex sugar systems. University of Canterbury, New Zealand.

Sun, Q., Li, Z., Li, S., Jiang, L., Wang, J., Wang, P. 2014. Utilization of surfactant-stabilized foam for enhanced oil recovery by adding nanoparticles. *Energy & Fuels*, 28: 2384–2394.

Takagi, S., Matsumoto, Y. 2011. Surfactant effects on bubble motion and bubbly flows. *Annual Review of Fluid Mechanics*, 43: 615–636.

Takagi, S., Ogasawara, T., Fukuta, M., Matsumoto, Y. 2009. Surfactant effect on the bubble motions and bubbly flow structures in a vertical channel. *Fluid Dynamics Research*, 41: 065003.

Telis, V. R. N., Telis-Romero, J., Mazzotti, H. B., Gabas, A. L. 2007. Viscosity of aqueous carbohydrate solutions at different temperatures and concentrations. *International Journal of Food Properties*, 10: 185–195.

Tripathi, M. K., Sahu, K. C., Karapetsas, G., Matar, O. K. 2015. Bubble rise dynamics in a viscoplastic material. *Journal of Non-Newtonian Fluid Mechanics*, 222: 217–226.

Ulaganathan, V., Krzan, M., Lotfi, M., Dukhin, S. S., Kovalchuk, V. I., Javadi, A., Gunes, D. Z., Gehin-Delval, C., Malysa, K., Miller, R. 2014. Influence of β-lactoglobulin and its surfactant mixtures on velocity of the rising bubbles. *Colloids and Surfaces A: Physicochemical and Engineering Aspects*, 460: 361–368.

Weller, H. G., Tabor, G., Jasak, H., Fureby, C. 1998. A tensorial approach to computational continuum mechanics using object-oriented techniques. *Computers in Physics*, 12: 620–631.

Zhang, C., Cheng, P., Cao, J. 2016. Mesoscale simulation of Marangoni convection about a vapor bubble in a liquid with temperature gradients under microgravity conditions. *International Communications in Heat and Mass Transfer*, 78: 295–303.

Zhang, J., Zhao, W., Liu, H., Xi, G. 2022. Numerical study of surfactant effects on the rise of a single bubble and two coaxial bubbles. *International Communications in Heat and Mass Transfer*, 137: 106284.

Ziegler, G. R., Benado, A. L., Rizvi, S. S. H. 1987. Determination of mass diffusivity of simple sugars in water by the rotating disk method. *Journal of Food Science*, 52: 501–502.